



NIH Public Access

Author Manuscript

Biochemistry. Author manuscript; available in PMC 2014 August 13.

Published in final edited form as:

Biochemistry. 2013 August 13; 52(32): . doi:10.1021/bi4007995.

Structural Insights into Fibrinogen Dynamics Using Amide Hydrogen/Deuterium Exchange Mass Spectrometry

James J. Marsh^{*†}, Henry S. Guan[†], Sheng Li, Peter G. Chiles, Danny Tran, and Timothy A. Morris

Department of Medicine, University of California at San Diego, La Jolla, California 92093.

Abstract

We determined the amide hydrogen/deuterium exchange profile of native human fibrinogen under physiologic conditions. After optimization of the quench and proteolysis conditions, more than 1,200 peptides were identified by mass spectrometry, spanning more than 90% of the constituent A, B, and C chain amino acid sequences. The compact central and distal globular regions of fibrinogen were well protected from deuterium exchange, with the exception of the unfolded amino-terminal segments of the A and B chains extending from the central region, and the short C chain “tail” extending from each distal globular region. The triple-helical coiled-coil regions, which bridge the central region to each distal region, were also well protected with the exception of a moderately fast-exchanging area in the middle of each coiled coil adjacent to the C chain carbohydrate attachment site. These dynamic regions appear to provide flexibility to the fibrinogen molecule. The C chain “out loop” contained within each coiled-coil also exchanged rapidly. The C domain (A 392–610) exchanged rapidly, with the exception of a short segment sandwiched between a conserved disulfide linkage in the N-terminal C subdomain. This latter finding is consistent with a mostly disordered structure for the C domain in native fibrinogen. Analysis of the dysfibrinogen B 235 Pro/Leu, which exhibits abnormal fibrin structure, revealed enhanced deuterium exchange surrounding the Pro/Leu substitution site as well as in the vicinity of the high affinity calcium binding site and the A knob polymerization pocket within the C domain. The implication of these changes with respect to fibrin structure is discussed.

Fibrinogen is a large, multi-domain protein found in the blood plasma of all vertebrate species. The protein is composed of three pairs of non-identical polypeptide chains termed A, B, and C, the predominant forms of which have 610, 461 and 411 amino acids, respectively, in circulating human fibrinogen.¹ During assembly fibrinogen also undergoes a number of post-translation modifications including addition of N-linked biantennary oligosaccharides at B Asn 364 and Asn 52, and non-stoichiometric phosphorylation of the A chain at Ser 3 and Ser 345.² Further heterogeneity results from common genetic polymorphisms at A 312 and B 448,³ and minor alternate splicing of transcripts encoding the A and C chains.²

The fibrinogen molecule has an elongated, triglobular shape and consists of several structural regions (see ref.⁴ for a detailed review of fibrinogen structure and function). Two

Copyright © American Chemical Society.

^{*}UCSD Medical Center, 200 West Arbor Drive, San Diego, CA 92103-8374. Telephone: 619-543-1944. jjmarsh@ucsd.edu.

[†]These authors contributed equally.

Supporting Information Available. Figures S1, S2, and S3; complete peptide coverage maps for the A, B, and C chains, respectively, of deuterated normal fibrinogen. Figures S4, S5, and S6; complete deuterium on-exchange profiles for the A, B, and C chains, respectively, of B 235 Pro/Leu and normal fibrinogen processed in parallel. This information is available free of charge via the Internet at <http://pubs.acs.org>.

terminal globular regions are each connected to a compact central domain by triple-helical coiled-coil segments. The amino-terminal segments of all six chains are gathered together in the central domain and secured by a network of disulfide bonds. Medial segments of the A₁, B₁ and C chains comprise each coiled-coil region. The distal globular regions each contain tightly folded domains from the C-terminal portions of the B₁ and C chains. The C-terminal portion of each A₁ chain departs from each distal region to form highly mobile C regions thought to interact with each other near the central domain.

The conversion of fibrinogen to fibrin results in its spontaneous polymerization and formation of a fibrin clot that prevents blood loss at sites of vascular injury. This process is initiated by the thrombin-catalyzed removal of short peptides from the amino-termini of the A₁ and B₁ chains. The newly exposed Gly-Pro-Arg (A knob) and Gly-His-Arg (B knob) sequences fit into ever-present “holes” on neighboring monomers to form half-staggered, two-molecule thick protofibrils, which laterally associate to form thick fibrin fibers.⁵ As polymerization proceeds, thrombin-activated factor XIII rapidly crosslinks neighboring chains, and more slowly, neighboring chains as well. The binding of the C-terminal portion of C chains to glycoprotein IIb-IIIa receptors on platelets, and the binding of RGD sequences to receptors on endothelial cells in vessel walls complete the clotting process. Polymerized fibrin also enhances tissue plasminogen activator-mediated conversion of plasminogen to plasmin, which triggers fibrinolysis by cleaving fibrin at specific sites within the coiled coils among others.

A high-resolution crystal structure of human fibrinogen has recently been published.⁶ Although many features of the molecule have been revealed in great detail, including the globular central and terminal domains as well as the triple helical coiled-coil segments, no resolvable electron density could be associated with the large C domains, suggesting that these regions are mostly disordered. Conversely, studies of recombinant C domains have demonstrated their ability to form soluble oligomers,⁷ and spectroscopic studies revealed that the C domains in these oligomers are folded into highly ordered compact structures.^{8,9}

Here we apply hydrogen/deuterium exchange detected by mass spectrometry (DXMS) to gain insights into the structure of native human fibrinogen in solution under physiologic conditions. The rate of hydrogen exchange at backbone peptide amide linkages has been used for many years as a sensitive probe for detecting changes in protein structure and dynamics.^{10,11} It is also useful for gaining insight into protein structure when x-ray crystallography is impractical due to either limited amounts of purified protein or inadequate crystal growth. The hydrogen exchange method is based on the fact that the rates at which amide hydrogen atoms in a protein exchange with deuterium in the bulk solvent are highly dependent on the protein’s conformation. Therefore, regions that are tightly folded into compact domains exchange slowly, while those that are more disordered or otherwise accessible to solvent exchange orders of magnitude faster. When the protein is subsequently fragmented by acid-stable proteases, DXMS can determine deuterium levels in short segments of the protein. The goals of the present study were to validate the technique by comparison of the deuterium exchange profile to the known crystal structure of human fibrinogen, and to gain further insights into regions not resolved in the crystal structure such as the C region, which comprises nearly two-thirds of the A₁ chain. We also provide an example of how the technique may be used to detect conformational changes in the fibrinogen variant B 235 Pro/Leu, which may account for its abnormal fibrin structure and function.

EXPERIMENTAL PROCEDURES

Materials

Fibrinogen was purified from citrated single-source human plasma by cold ethanol precipitation as previously described.¹² Fibrinogen stock solutions (4.0 mg/ml in 20 mM sodium citrate, 150 mM NaCl, pH 7.0) were divided into small aliquots and stored at -70°C. Human fibrinogen conjugated with Alexa Fluor 488 (9 moles dye/mole protein) was purchased from Molecular Probes (Grand Island, NY). Human α -thrombin (2,997 NIH units/mg) and gluplasminogen were purchased from Enzyme Research Laboratories (South Bend, IN). Recombinant human tissue-type plasminogen activator (tPA) was obtained from Burroughs Wellcome (Research Triangle Park, NC). Porcine pepsin (3,200–4,500 units/mg protein), fungal protease from *Aspergillus saitoi* (type XIII), and tris(2-carboxyethyl)phosphine hydrochloride (TCEP) were purchased from Sigma (St. Louis, MO). The proteases were coupled to Poros AL- 20 μ m resin (Life Technologies, Grand Island, NY) at 30 mg /ml resin according to the manufacturer's instructions. C18 trap columns (MAGIC C18AQ, 0.2 \times 2 mm) and C18 analytical columns (MAGIC C18AQ 3 μ 200 Å, 0.2 \times 50 mm) were purchased from Bruker-Michrom (Auburn, CA). Deuterated water (D_2O) was obtained from Cambridge Isotope Laboratories (Andover, MA).

Characterization of normal fibrinogen

Fibrinogen purity was assessed by SDS PAGE on 4–12% Bis-Tris polyacrylamide gels (Life Technologies) under reducing and non-reducing conditions after staining with Colloidal Blue (Life Technologies). Percent clottable protein was determined by measuring the UV absorbance ($\lambda = 280$ nm) of the fibrinogen solution (1 mg/ml) before and after clotting with thrombin (0.5 NIH units/ml) in the presence of 10 mM CaCl₂, after removal of the fibrin clot by centrifugation. DNA sequencing of the fibrinogen genes *FGA*, *FGB*, and *FGG* as well as liquid chromatography-mass spectrometry of purified fibrinogen were performed as previously described.¹³ Identification and characterization of the B 235 Pro/Leu fibrinogen variant has been described elsewhere.¹³

Establishment of optimal proteolysis conditions

Prior to conducting hydrogen/deuterium exchange experiments, test samples of normal fibrinogen were prepared in non-deuterated buffer containing various concentrations of guanidine HCl and TCEP to determine optimal proteolysis conditions. A sample of fibrinogen stock solution (12 μ l) was diluted in 36 μ l of H₂O buffer (8.3 mM Tris, 150 mM NaCl, pH 7.16). Aliquots (8 μ l) were mixed with 12 μ l of a quench solution containing various concentrations of guanidine HCl (0.5–6.4 M) and TCEP (0.05 M or 1.0 M) in 0.76% (v/v) formic acid. The quench solution denatures the protein, reduces disulfide bonds, and lowers the pH to slow the rate of amide hydrogen/deuterium back-exchange. After incubating on ice for 5 min, the samples were diluted 8-fold with 0.76% (v/v) formic acid containing 16.6% (v/v) glycerol, and then frozen at -80°C for further analysis. This dilution step reduced the concentrations of denaturant and reducing agent to levels that did not adversely affect the activity of the proteolytic enzymes used for subsequent fragmentation of the protein.

When ready for proteolysis and mass spectrometry, the samples were thawed at 4°C and applied to one of three protease column configurations (16 μ l bed volume) at 0°C: (1) pepsin alone, (2) fungal protease alone, or (3) pepsin and fungal protease columns connected, respectively, in tandem. Proteolytic fragments were eluted at 20 SI/min and collected on a C18 trap column at 0°C. The peptides were separated on a C18 reversed phase analytical column at 0°C using a linear gradient of 0.046% (v/v) trifluoroacetic acid, 6.4% (v/v) acetonitrile to 0.03% (v/v) trifluoroacetic acid, 38.4% (v/v) acetonitrile over 30 min with the

column effluent directed into an Orbitrap Elite Mass Spectrometer (ThermoFisher Scientific, San Jose, CA). The instrument was operated in the positive ESI mode with a sheath gas flow of 8 units, a spray voltage of 4.5 kV, a capillary temperature of 200°C, and an S-lens RF of 67%. Mass spectroscopy data were acquired in both MS1 profile mode and data-dependent MS1:MS2 mode. The resolution of the survey scan was set at 60,000, at m/z 400 with a target value of 1×10^6 ions and 3 microscans. The maximum injection time for MS/MS fragmentation was varied between 25 and 200 ms. Dynamic exclusion was 30 s and early expiration was disabled. The isolation window for MS/MS fragmentation was set to 2, and the five most abundant ions were selected for product ion analysis. Proteome Discoverer software (ThermoFisher) was used to identify the sequence of the peptide ions.

On-exchange protein deuteration

Once the optimal proteolysis conditions were determined, functional deuteration of fibrinogen was performed by diluting 12 µl of fibrinogen stock into 36 µl of D₂O buffer (8.3 mM Tris, 150 mM NaCl in D₂O, pH 7.16) at 0°C. Then, at 10, 30, 100, 300, 1,000, 3,000, and 10,000 seconds an aliquot (6 µl) was removed and quenched with 9 µl of 0.76% (v/v) formic acid containing 6.4 M guanidine HCl and 1.0 M TCEP. After 5 min on ice, the quenched samples were diluted and frozen at -80°C as described above. In addition, non-deuterated samples (incubated in H₂O buffer) and equilibrium-deuterated samples (incubated in D₂O buffer containing 0.8% (v/v) formic acid for 24 h at 25°C) were prepared. All samples subsequently underwent proteolysis with both pepsin and fungal proteases followed by mass spectrometry analysis as described above. The centroids of the isotopic envelopes of nondeuterated, functionally-deuterated and equilibrium-deuterated peptides were measured using DXMS Explorer software (Sierra Analytics, Modesto, CA). The deuteration levels of the functionally-deuterated peptides were calculated relative to the corresponding peptides from the equilibrium-deuterated samples, the latter of which were taken as a maximum deuteration level of 100%.¹⁴

Fibrin clot polymerization, lysis, and permeability

Fibrin clots from B-235 Pro/Leu and normal fibrinogen were simultaneously formed and lysed as previously described.¹³ Briefly, each type of fibrinogen was mixed with plasminogen, tPA and thrombin in 50 mM Tris (pH 7.0) containing 150 mM NaCl and 10 mM CaCl₂. The mixture was immediately added to a microplate well and the turbidity of the solution was continuously monitored in a microplate reader for one hour. Each curve was characterized by an increase in absorbance (polymerization) followed by a brief plateau and then a decrease in absorbance (lysis) to baseline. Lysis rates were calculated from the slope of the lysis portion of each curve at 50% maximum turbidity. Fibrin clot permeability was assessed using a modification of a previously described method.¹⁵ Briefly, fibrin clots were formed as described above except that plasminogen and tPA were omitted. The clot mixture (300 µl) was immediately added to a disposable 1-ml column that had been previously primed with de-aerated permeation buffer (50 mM Tris (pH 7.0) containing 150 mM NaCl and 0.1% (w/v) bovine serum albumin) and sealed at the bottom with parafilm. The column was placed in a humid chamber for 2 hours at room temperature. Flow measurements were performed at constant hydrostatic pressure and the Darcy constant K_s was calculated from the flow rate of buffer through the clot, which is directly related to the pore size of the fibrin network.

Confocal microscopy of fibrin clots

Fibrin clots were formed as described above for permeation studies except that Alexa Fluor 488-conjugated fibrinogen was added (10% final fibrinogen concentration) to enable visualization of fibrin fibers. The clot mixture (100 µl) was immediately added to duplicate wells of a glass bottom 96-well plate (MatTek Corp., Ashland, MA) and incubated for 2

hours at room temperature in a humid chamber. Fibrin networks were visualized with an Olympus FV1000 inverted laser-scanning confocal microscope equipped with a 100X (1.4 numerical aperture) objective and controlled by FlowView software (version 3.0.2.0). Images were collected in the XYZ scan mode using 3% laser power with filters automatically set for detection of Alexa Fluor 488. Image size was 512x512 pixels in the XY dimension (0.248 $\mu\text{m}/\text{pixel}$), and 41 optical sections were collected in the Z dimension (0.38 $\mu\text{m}/\text{slice}$). Care was taken to start the optical sectioning of each clot approximately 35 μm from the surface of the cover glass, with subsequent sections penetrating deeper into the clot. Fully reconstructed images were used for visual analysis. NIH ImageJ software (version 1.45) was used to estimate fiber diameter and the extent of fiber branching by an operator blinded to the identity of the samples.

RESULTS

Characterization of fibrinogen

The normal fibrinogen preparation was >95% pure as judged by SDS PAGE (Fig. 1A) and contained $94.1 \pm 0.3\%$ clottable protein (mean \pm SD, n=3). Typical heterogeneity of the A chain¹⁶ as well as trace amounts of the C chain¹⁷ were observed. DNA sequencing of the fibrinogen genes and standard liquid chromatograph-mass spectrometry analysis of the fibrinogen chains disclosed normal fibrinogen structure, including common alleles at polymorphic sites A 312 and B 448 (Fig. 1B). Detailed characterization of the B 235 Pro/Leu fibrinogen variant has been described elsewhere.¹³

Optimization of proteolytic fragmentation of normal fibrinogen

Prior to performing deuterium exchange experiments, the condition that produced optimal fragmentation and recovery of identifiable peptides from all three fibrinogen chains was determined by varying the concentrations of guanidine HCl and TCEP in the quench solution and by varying the protease(s) used for fragmentation. The goal was to obtain a large number of overlapping peptides that spanned the entire amino acid sequence of each chain. The results of a typical experiment using a quench solution with low (0.5 M) guanidine HCl and low (0.05 M) TCEP followed by proteolysis with either pepsin, or fungal protease, or a combination of both proteases are presented in Table 1. Pepsin alone gave reasonably good fragmentation of all three chains, but very few peptides were recovered from a large portion of the C region. The peptides spanned 93.4%, 89.2%, and 87.6 % of the A, B, and C chain amino acid sequences, respectively. Compared to pepsin, the fungal protease produced fewer peptides, especially in the B and C chains, and significant coverage gaps were observed in the coiled-coil regions of all three chains. However, the fungal protease gave a much higher density of peptides in the C region compared to pepsin. The greatest number of peptides and the best coverage for all three chains was achieved when both pepsin and fungal proteases were used in tandem (Table 1). It was noted that some coverage gaps in all three chains occurred in cysteine-rich regions known to be involved in disulfide bonding (A 156–168, B 67–81, B 191–198, and C 132–142). As shown in Table 2, increasing the concentration of TCEP and guanidine HCl in the quench solution to 1.0 M and 6.4 M, respectively, substantially increased the number of peptides recovered from the A and B chains; in addition, the aforementioned coverage gaps in the B and C chains were eliminated and resulted in >90% coverage for all three chains (Table 2). Neither the number of peptides recovered nor the coverage was improved by using other concentrations of guanidine HCl and TCEP in the quench solution (data not shown). Therefore, the optimized conditions used in the deuterium exchange experiments described below included a quench solution containing 6.4 M guanidine HCl and 1.0 M TCEP, and fragmentation with both pepsin and fungal proteases.

Deuterium on-exchange profile of normal fibrinogen

To assess the deuterium exchange profile of normal fibrinogen, the protein was incubated in deuteration buffer for 10–10,000 s at 0°C and then quenched with a low-pH buffer to slow the back-exchange rate during subsequent analysis. In addition, non-deuterated and equilibrium-deuterated sets were prepared. The extent of deuterium incorporation at each time point was determined by mass spectrometry and reported as percent deuteration as described in Experimental Procedures. To be included in the deuteration profile, each peptide had to be identified in the non-deuterated, functionally-deuterated (all time points), and equilibrium-deuterated states. This resulted in fewer peptides plus additional and/or larger gaps than were previously observed in the optimization experiments. An abbreviated coverage map showing peptides satisfying the deuteration profile criteria is shown in Figure 2. This abbreviated map is designed to show the extent of coverage across the complete amino acid sequence for each chain, but does not include all of the recovered peptides. (Complete deuteration profile coverage maps for the A₁, B₁, and C chains are presented as Figs. S1, S2, and S3, respectively, in Supporting Information.) For the A₁ chain, 309 peptides covering 81.6% of the amino acid sequence were identified. Substantial gaps at A₁ 145–174 and A₁ 270–347 were consistently observed regardless of the quench conditions employed or the protease(s) used for fragmentation (Fig. 2A); however, full coverage and high peptide density were observed in the C domain (A₁ 392–610). For the B₁ chain, 224 peptides were identified covering 89.8% of the amino acid sequence. Because Proteome Discoverer software is not able to identify peptides to which complex carbohydrates are attached, the gap at B₁ 361–374 was expected due to the carbohydrate attachment site at B₁ Asn 364 (Fig. 2B). For the C chain, 177 peptides were identified covering 87.8% of the amino acid sequence. As shown in Figure 2C, two gaps were consistently observed (A₁ 48–65 and A₁ 142–154). The former gap was expected due to the carbohydrate attachment site at Asn 52. The A₁-, B₁- and C-chain deuterium exchange profiles are presented in Figures 3, 4, and 5, respectively, and will be described in terms of the fibrinogen regions the chains comprise in the sections below.

Central region

The amino-terminal segments of the A₁ and B₁ chains (A₁ 1–26 and B₁ 1–54) extending from the compact central domain were fully deuterated within 10 seconds (Figs. 3, 4). These segments, which do not resolve in the crystal structure, include the fibrinopeptides A and B, respectively. The compact part of the domain includes segments from pairs of all three chains (A₁ 27–49, B₁ 58–80, and C 14–23), which are held together by 11 disulfide bonds. These segments were well protected from deuterium exchange (Figs. 3–5).

Coiled-coil region

The triple-helical coiled-coil region includes segments from all three chains (A₁ 50–160, B₁ 81–192, and C 24–134), and is delimited at each end by a set of disulfide rings. Whereas the deuteration profile was slow-exchanging at either end of the coiled coil, relatively fast-exchanging segments were observed near the middle of all three chains in the vicinity of plasmin cleavage sites (Figs. 3–5). A large gap in the deuteration profile of the A₁ chain at the distal end of the coiled coil (A₁ 145–176; Fig. 3) was consistently observed. As mentioned previously, the gap at A₁ 48–67 was anticipated due to the carbohydrate attachment site at C Asn 52 (Fig. 5).

Distal globular region

The globular region at each end of the fibrinogen molecule is made up of tightly folded C and C globular domains. The A₁ chain makes an abrupt turn at the end of the coiled coil and then forms a fourth helix running opposite to the direction of the three-stranded

coil.^{6, 18, 19} Of note, the segment corresponding to the fourth helix (A 175–190) was well protected from deuterium exchange (Fig. 3). The segment comprising the C domain (B 194–461) exchanged slowly, although a short segment (B 386–392) became fully deuterated within 5 minutes (Fig. 4). This latter segment is in close proximity to the B knob polymerization pocket. Once again, the gap at B 361–376 was anticipated because of the carbohydrate attachment site at B Asn 364. The segment comprising the C domain (136–394) was also well protected, although several short segments became highly deuterated upon prolonged incubation (Fig. 5). One segment (319–326) is in close proximity to a high-affinity calcium binding site, while two others (296–303 and 350–359) are in the vicinity of the A knob polymerization pocket. The chain “tail” extending from the globular domain, which includes the glutamine and lysine residues involved in factor XIIIa-catalyzed crosslinking, was fast exchanging and did not resolve in the crystal structure.

αC region

The C region (A 221–610) consists of a compact domain (A 392–610) and a flexible connector (A 221–391) that tethers the entire region to the rest of the fibrinogen molecule. As shown in Figure 3, the deuterium exchange profile revealed that the segment between the fourth helix and the C connector (A 191–220) was well protected in the middle but relatively fast exchanging at either end. An early plasmin cleavage site is contained within this segment. With the exception of a short rather slow-exchanging segment at A 228–240, the C connector was fully deuterated within 10 seconds. However, a large gap at A 270–349 was consistently observed, precluding any definitive conclusions regarding the folding behavior of this segment. Of note, this gap included a series of 13-residue imperfect tandem repeats beginning at A 264.²⁰

The entire C domain (A 392–610) was very fast exchanging, suggesting a mostly disordered structure. Many overlapping peptides were identified in this region (Fig. 3), implying that even short segments of ordered structure should have been detected. In this regard, a slightly more protected segment (A 450–462) was found within the N-terminal C subdomain (A 425–503) precisely where some core structure has been previously identified using NMR techniques.⁹

Association of deuteration profile with crystal structure

To illustrate how well the deuteration profile of all three pairs of chains corresponded to the known crystal structure of human fibrinogen, a ribbon model of the protein was color-coded according to the deuteration profile of each chain (Fig. 6A). The 10-second deuteration time point was chosen for this representation because it seemed to show the broadest spectrum of deuteration levels across the entire amino acid sequence of each chain. For reference, the same model, color-coded by chain, is shown in Figure 6B. In general, there was a very good concordance between the deuteration profile and the crystal structure. The tightly folded C and C domains of the terminal globular regions were well protected from deuterium exchange (Fig. 6C, mostly blue, <25% deuteration). The -helices comprising the three-stranded coiled-coil regions bridging the central and terminal regions were also slow exchanging with three notable exceptions: an 18-residue loop extending from the chain in the middle of the coiled coil (Fig. 6D, red, >90% deuteration), and two short juxtaposed -helical segments in the A and B chains slightly upstream from the chain loop (Fig. 6D, yellow, >75% deuteration). Unfortunately, the deuteration profile of the chain in this dynamic region could not be ascertained due to the presence of the carbohydrate attachment site. Despite a general lack of much secondary structure, the segments of the A, B, and chains comprising the small tightly folded central region were fairly well protected from deuterium exchange (Fig. 6E).

Structural properties of B β 235 Pro/Leu fibrin clots

We previously reported a high prevalence of the dysfibrinogen B 235 Pro/Leu among a cohort of patients with chronic thromboembolic pulmonary hypertension.¹³ As shown in Figure 7A, fibrin clots formed from B 235 Pro/Leu fibrinogen exhibited a markedly lower maximal turbidity and lysis rate compared to normal fibrin (Table 3). In addition, the B 235 Pro/Leu fibrin network (Fig. 7B) had a more disorganized structure compared to normal fibrin (Fig. 7C) characterized by thinner fibers, greater network branching (Table 3), and visibly smaller pores. In agreement with the latter observation, the Darcy constant K_s (a direct measure of network pore size) of B 235 Pro/Leu fibrin was substantially lower compared to normal fibrin as determined from clot permeation studies (Table 3).

Deuterium on-exchange profile of B β 235 Pro/Leu fibrinogen

To determine whether the B 235 Pro/Leu substitution, which occurs at the interface between the globular C and C domains (Fig. 8), results in a conformational change that might contribute to the abnormal fibrin structure, the deuterium exchange profile of the variant was determined in parallel with normal fibrinogen. The complete deuteration profiles of the A, B, and chains of both proteins are presented as Figures S4, S5, and S6, respectively, in Supporting Information. The deuteration profiles of the A chain of both proteins were very similar. While the deuteration profiles of the B chain of both proteins were also quite similar, the variant showed moderately enhanced deuterium exchange in a segment (B 226–235) immediately preceding the B 235 substitution site (Figs. 8 and 9). Somewhat surprisingly, several segments within the C domain of the variant showed markedly enhanced deuterium exchange compared to the normal protein (Fig. 10). One segment (319–326), which is in close proximity to the C calcium binding site (Fig. 8), was fully deuterated within 10 seconds. Two other segments (291–303 and 350–366), which form the walls of the A knob polymerization pocket (Fig. 8), were >85% deuterated within 100 seconds. It is also noteworthy that although there were some differences in the peptides produced, the deuteration profiles of the normal protein from separate experiments were remarkably similar, demonstrating the reproducibility of the technique (compare Figs. 3, 4, 5 and S4, S5, S6, respectively).

DISCUSSION

In the present study, we used DXMS to gain insights into the structure and dynamics of native human fibrinogen in solution under physiologic conditions, focusing in particular on regions that do not resolve in the crystal structure such as the C domain. With a total of 1,482 amino acid residues in each set of three polypeptide chains, and 29 inter- and intra-chain disulfide bonds, fibrinogen is arguably one of the largest and most structurally complex proteins to be analyzed by DXMS thus far. After optimization of the quench and proteolysis conditions, more than 1,200 peptides were identified, spanning over 90% of the amino acid sequence of all three chains. For regions that resolve in the crystal structure, the deuteration profile of all three chains was, for the most part, slow-exchanging as expected. One notable exception was a very fast-exchanging segment in the middle of the coiled-coil region (68–78), which coincided precisely with the chain “out-loop” in the crystal structure (Fig. 6D). A similar departure from helicity occurs at virtually the same location in the chain from other species.^{18, 19} Another intriguing area within the coiled coil involved two relatively fast-exchanging, juxtaposed segments (A 81–86 and B 108–116) slightly upstream of early plasmin cleavage sites (Figs. 6A and 6D). These segments are composed of runs of polar amino acids rarely seen in -helices. Unfortunately, the deuteration behavior of the neighboring chain segment could not be ascertained due to the presence of the chain carbohydrate attachment site. This dynamic region, seen for the first time in native fibrinogen under physiologic conditions, coincides with the “flexible hinge” originally

proposed based on crystal structure alignments within the coiled-coil region of fibrinogens from various species.^{6, 18, 19} This pivot point is believed to provide flexibility to individual molecules as well as to fibrin strands. This region is also a “touch point” where the coiled coils from different molecules associate in an anti-parallel fashion in the crystal structure,⁶ these kinds of associations may also occur in fibrin as a part of the polymerized network organization. It is noteworthy that fibrinogen Caracas VI, which lacks A Asn-80,²¹ and fibrinogen Kyoto IV, which lacks B Ser-111,²² both exhibit defective fibrin network organization.

The structure of the hydrophilic C region has long been a matter of debate.²³ According to the popular view, the C domains in fibrinogen interact *intra-molecularly* near the central domain, while in fibrin, they interact *inter-molecularly* to form C polymers, which are covalently cross-linked by factor XIIIa.^{4, 24} The switch from intra- to inter-molecular interactions is facilitated by the removal of fibrinopeptides from the central region and by the intrinsic flexibility of the C connector region. The C domain was first visualized by electron microscopy^{25, 26} and was characterized as an independent folding unit by calorimetry.^{27, 28} More recent spectroscopic studies with recombinant C fragments predict a compact globular structure for the C domain.^{7, 9, 29} However, other evidence, including sensitivity to a variety of proteases,²⁰ a rapid rate of evolutionary change,³⁰ and the absence of any discernible structure in electron density maps from X-ray diffraction data^{6, 19} has supported the conclusion that the C region, including C domain, is mostly disordered. Our deuterium exchange data with native fibrinogen under physiologic conditions appears to favor a mostly disordered structure for the C domain, with essentially the entire region exchanging within the same time frame as the unfolded amino-terminal segments of the A and B chains. However, detection of subtle regions of organized structure may require DXMS analysis using the flow quench approach,³¹ which involves rapid mixing of the protein with D₂O so that mixing and quench steps can be accomplished within milliseconds.

NMR studies with recombinant fragments representing full length and truncated bovine C domains have detected the presence of two -hairpins forming a mixed parallel/antiparallel -sheet in the N-terminal C subdomain.⁷ A similar structure representing the first but not the second -hairpin was found in the human counterpart.⁹ The sequences from bovine and human species in the area of the first -hairpin (and anti-parallel -sheet) are sandwiched between a highly-conserved disulfide linkage (Cys 442 and Cys 472 in human fibrinogen) and display more than 90% homology, implying a nearly identical fold.⁹ Interestingly, our experiments with native fibrinogen revealed a short segment slightly more protected from deuterium exchange (A 450–462) within this region (Fig. 3).

DXMS has been increasingly applied to the study of intrinsically disordered proteins and intrinsically disordered regions within otherwise structured proteins.³² Some such proteins are only unfolded until they find their binding partner, and then fold upon binding, which is reflected by a change in the protein’s deuterium exchange profile.^{33–35} Many other intrinsically disordered proteins tend to aggregate or undergo oligomer formation, which is accompanied by a shift to a more ordered structure.^{36, 37} This latter behavior is reminiscent of the oligomer formation that occurs with recombinant C domains,^{7–9} and may contribute to C polymer formation in native fibrin as well. DXMS offers an attractive opportunity to study these structural transitions in more detail using recombinant C fragments as well as soluble native fibrin oligomers.³⁸

We have recently identified several dysfibrinogenemias associated with chronic thromboembolic pulmonary hypertension.¹³ These fibrinogen variants result from heterozygous missense mutations leading to non-conservative amino acid substitutions in one or more of the fibrinogen chains. All are associated with abnormal fibrin clot structure

and delayed fibrinolysis. Two of these variants have mutations affecting the coiled-coil region: one at the proximal end (A 69 Leu/His) and one at the distal end (114 Tyr/His). Another variant has a mutation affecting tightly folded C domain in the distal globular region. In this case, a highly-conserved proline residue is replaced with leucine at residue 235 of the B chain. The deuterium exchange profile surrounding each of these sites is now well characterized, and in each case was found to be very slow exchanging. In the present study we have applied DXMS to determine the deuterium exchange profile of B 235 Pro/Leu fibrinogen. Somewhat surprisingly, substitution of the conformationally restrained proline residue with leucine at the interface between the C and C domains resulted in markedly enhanced deuterium exchange in the vicinity of the calcium binding site (319–326) and the A knob polymerization pocket (291–303 and 350–366) within the C domain (Fig. 8). Dynamic changes in this region might be expected to alter fibrin structure and susceptibility to fibrinolysis. In this regard, lateral association of protofibrils, which is the basis of clot turbidity, is affected by calcium ion concentration.^{39, 40} A less ordered structure could lower the affinity of the calcium ion for its ligands and thereby contribute to the production of more transparent clots with thinner fibers. The 319–326 segment is also part of a region (312–324) that has been implicated in tPA binding,⁴¹ therefore, dynamic changes in this region might also alter plasminogen activation and fibrinolysis.

In summary, DXMS shows promise for obtaining information on the structure and dynamics of native fibrinogen currently lacking with other high-resolution methods. The technique may therefore be useful for understanding structural changes that occur during fibrin polymer assembly, and for probing the structure of clinically relevant fibrinogen variants for perturbations in the folding behavior surrounding the affected site(s). This in turn may provide insights into structure/function relationships of fibrinogen and fibrin in health and in thrombotic diseases.

Supplementary Material

Refer to Web version on PubMed Central for supplementary material.

Acknowledgments

We would like to dedicate this manuscript to our mentor and colleague, Dr. Virgil L. Woods, Jr. who passed away during the course of this investigation. Dr. Woods was an expert in deuterium exchange mass spectroscopy and most of this work was conducted in his laboratory. His enthusiastic support, vast knowledge, and general oversight were critical to the success of the project. We also wish to acknowledge the efforts of Dr. Ni-Cheng Liang and Jun Ho Lee for their efforts during the early phases of the project. We also thank Dr. Russell Doolittle for helpful discussions along the way and for his critical reading of the manuscript.

This work was supported by grants HL095089 and GM093325 from the National Institutes of Health.

ABBREVIATIONS

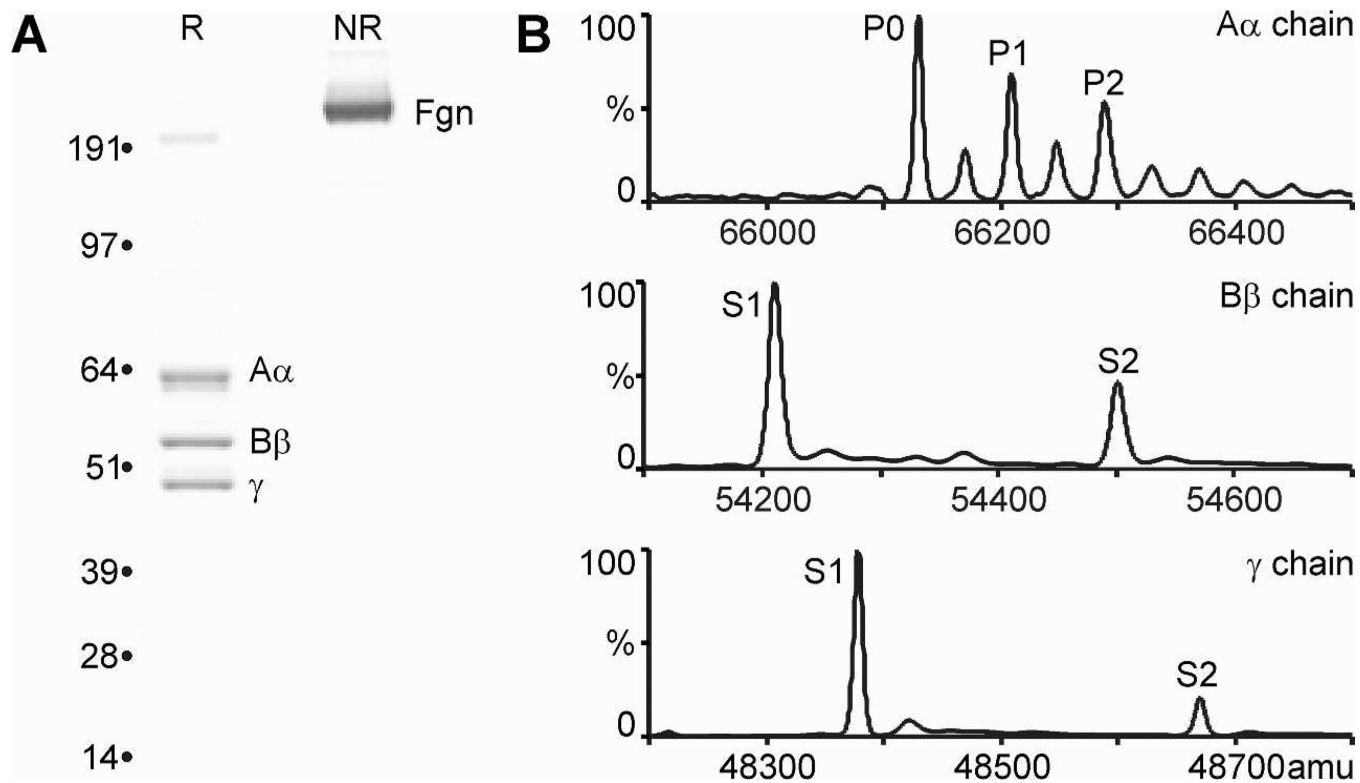
DXMS	hydrogen/deuterium exchange detected by mass spectrometry
tPA	tissue-type plasminogen activator
D₂O	deuterated water
TCEP	tris(2-carboxyethyl)phosphine hydrochloride
NMR	nuclear magnetic resonance
CD	circular dichroism.

REFERENCES

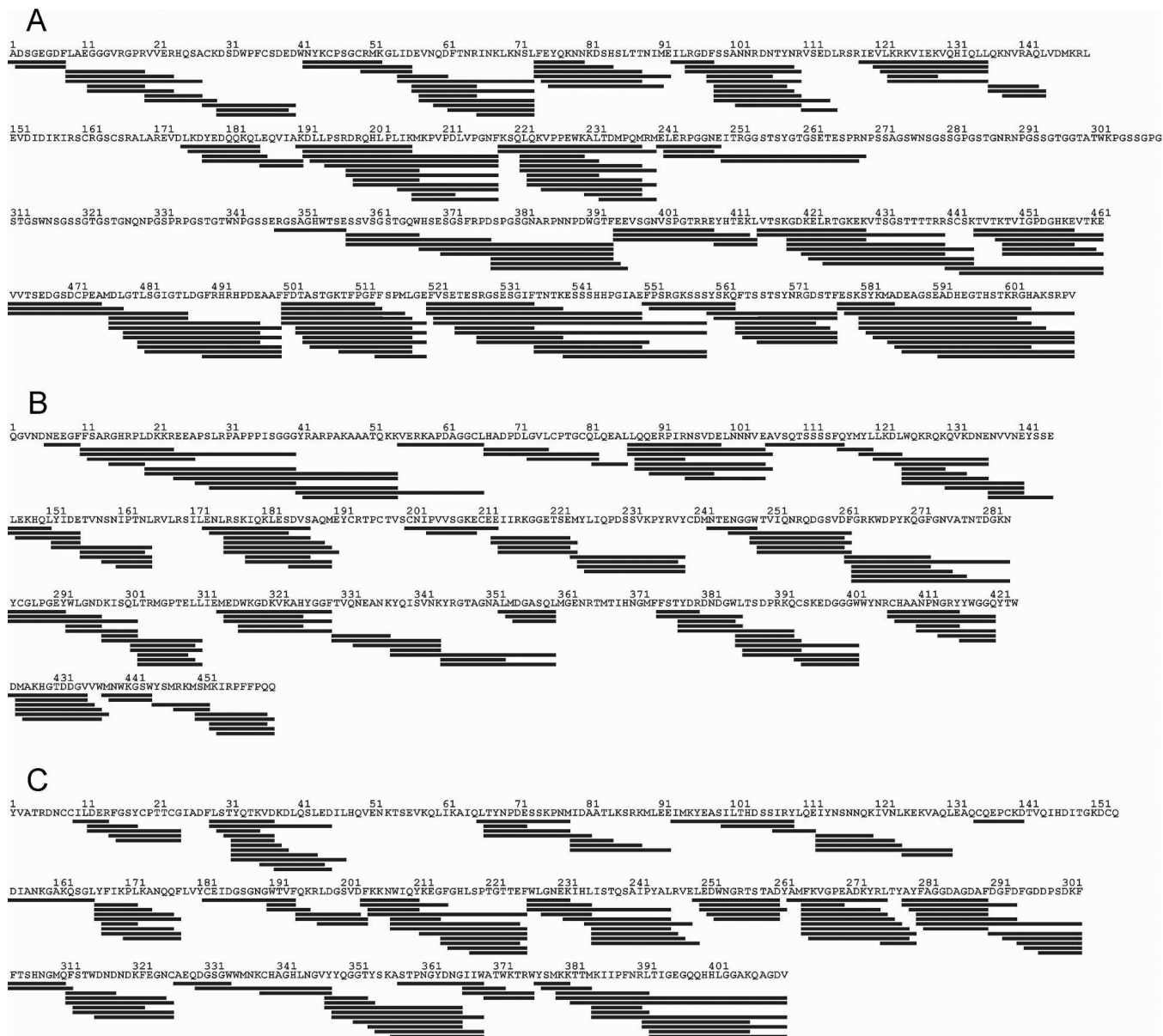
1. Henschen A, Lottspeich F, Kehl M, Southan C. Covalent structure of fibrinogen. *Ann N Y Acad Sci.* 1983; 408:28–43. [PubMed: 6575689]
2. Henschen-Edman AH. Fibrinogen non-inherited heterogeneity and its relationship to function in health and disease. *Ann N Y Acad Sci.* 2001; 936:580–593. [PubMed: 11460517]
3. Baumann RE, Henschen AH. Human fibrinogen polymorphic site analysis by restriction endonuclease digestion and allele-specific polymerase chain reaction amplification: Identification of polymorphisms at positions A 312 and B 448. *Blood.* 1993; 82:2117–2124. [PubMed: 8400261]
4. Mosesson MW. Fibrinogen and fibrin structure and functions. *J Thromb Haemost.* 2005; 3:1894–1904. [PubMed: 16102057]
5. Blomback B, Hessel B, Hogg D, Therkildsen L. A two-step fibrinogen–fibrin transition in blood coagulation. *Nature.* 1978; 275:501–505. [PubMed: 692730]
6. Kollman JM, Pandi L, Sawaya MR, Riley M, Doolittle RF. Crystal structure of human fibrinogen. *Biochemistry.* 2009; 48:3877–3886. [PubMed: 19296670]
7. Burton RA, Tsurupa G, Hantgan RR, Tjandra N, Medved L. NMR solution structure, stability, and interaction of the recombinant bovine fibrinogen C-domain fragment. *Biochemistry.* 2007; 46:8550–8560. [PubMed: 17590019]
8. Tsurupa G, Mahid A, Veklich Y, Weisel JW, Medved L. Structure, stability, and interaction of fibrin C-domain polymers. *Biochemistry.* 2011; 50:8028–8037. [PubMed: 21806028]
9. Tsurupa G, Hantgan RR, Burton RA, Pechik I, Tjandra N, Medved L. Structure, stability, and interaction of the fibrin(ogen) C-domains. *Biochemistry.* 2009; 48:12191–12201. [PubMed: 19928926]
10. Englander SW, Kallenbach NR. Hydrogen exchange and structural dynamics of proteins and nucleic acids. *Q Rev Biophys.* 1983; 16:521–655. [PubMed: 6204354]
11. Wales TE, Engen JR. Hydrogen exchange mass spectrometry for the analysis of protein dynamics. *Mass Spectrom Rev.* 2006; 25:158–170. [PubMed: 16208684]
12. Doolittle RF, Schubert D, Schwartz SA. Amino acid sequence studies on artiodactyl fibrinopeptides. I. Dromedary camel, mule deer, and cape buffalo. *Arch Biochem Biophys.* 1967; 118:456–467. [PubMed: 6033721]
13. Morris TA, Marsh JJ, Chiles PG, Magana MM, Liang NC, Soler X, Desantis DJ, Ngo D, Woods VL Jr. High prevalence of dysfibrinogenemia among patients with chronic thromboembolic pulmonary hypertension. *Blood.* 2009; 114:1929–1936. [PubMed: 19420351]
14. Zhang Z, Smith DL. Determination of amide hydrogen exchange by mass spectrometry: A new tool for protein structure elucidation. *Protein Sci.* 1993; 2:522–531. [PubMed: 8390883]
15. Collet JP, Soria J, Mirshahi M, Hirsch M, Dagonnet FB, Caen J, Soria C. Dusart syndrome: A new concept of the relationship between fibrin clot architecture and fibrin clot degradability: Hypofibrinolysis related to an abnormal clot structure. *Blood.* 1993; 82:2462–2469. [PubMed: 7691261]
16. Cottrell BA, Doolittle RF. The amino acid sequence of a 27-residue peptide released from the -chain carboxy-terminus during the plasmic digestion of human fibrinogen. *Biochem Biophys Res Commun.* 1976; 71:754–761. [PubMed: 134710]
17. Cooper AV, Standeven KF, Ariens RA. Fibrinogen gamma-chain splice variant ' alters fibrin formation and structure. *Blood.* 2003; 102:535–540. [PubMed: 12663453]
18. Brown JH, Volkmann N, Jun G, Henschen-Edman AH, Cohen C. The crystal structure of modified bovine fibrinogen. *Proc Natl Acad Sci U S A.* 2000; 97:85–90. [PubMed: 10618375]
19. Yang Z, Kollman JM, Pandi L, Doolittle RF. Crystal structure of native chicken fibrinogen at 2.7 Å resolution. *Biochemistry.* 2001; 40:12515–12523. [PubMed: 11601975]
20. Doolittle RF, Watt KW, Cottrell BA, Strong DD, Riley M. The amino acid sequence of the -chain of human fibrinogen. *Nature.* 1979; 280:464–468. [PubMed: 460425]
21. Marchi RC, Meyer MH, de Bosch NB, Arocha-Pinango CL, Weisel JW. A novel mutation (deletion of A -Asn 80) in an abnormal fibrinogen: Fibrinogen Caracas VI. Consequences of disruption of the coiled coil for the polymerization of fibrin: Peculiar clot structure and diminished stiffness of the clot. *Blood Coagul Fibrinolysis.* 2004; 15:559–567. [PubMed: 15389122]

22. Okumura N, Terasawa F, Hirota-Kawadobora M, Yamauchi K, Nakanishi K, Shiga S, Ichiyama S, Saito M, Kawai M, Nakahata T. A novel variant fibrinogen, deletion of B 111Ser in coiled-coil region, affecting fibrin lateral aggregation. *Clin Chim Acta*. 2006; 365:160–167. [PubMed: 16229829]
23. Doolittle RF, Kollman JM. Natively unfolded regions of the vertebrate fibrinogen molecule. *Proteins*. 2006; 63:391–397. [PubMed: 16288455]
24. Weisel JW, Medved L. The structure and function of the C domains of fibrinogen. *Ann N Y Acad Sci*. 2001; 936:312–327. [PubMed: 11460487]
25. Mosesson MW, Hainfeld J, Wall J, Haschemeyer RH. Identification and mass analysis of human fibrinogen molecules and their domains by scanning transmission electron microscopy. *J Mol Biol*. 1981; 153:695–718. [PubMed: 7338923]
26. Erickson HP, Fowler WE. Electron microscopy of fibrinogen, its plasmic fragments and small polymers. *Ann N Y Acad Sci*. 1983; 408:146–163. [PubMed: 6575682]
27. Privalov PL, Medved LV. Domains in the fibrinogen molecule. *J Mol Biol*. 1982; 159:665–683. [PubMed: 7143446]
28. Medved LV, Gorkun OV, Privalov PL. Structural organization of C-terminal parts of fibrinogen A -chains. *FEBS Lett*. 1983; 160:291–295. [PubMed: 6224704]
29. Burton RA, Tsurupa G, Medved L, Tjandra N. Identification of an ordered compact structure within the recombinant bovine fibrinogen C-domain fragment by NMR. *Biochemistry*. 2006; 45:2257–2266. [PubMed: 16475814]
30. Murakawa M, Okamura T, Kamura T, Shibuya T, Harada M, Niho Y. Diversity of primary structures of the carboxy-terminal regions of mammalian fibrinogen A -chains. Characterization of the partial nucleotide and deduced amino acid sequences in five mammalian species; rhesus monkey, pig, dog, mouse and syrian hamster. *Thromb Haemost*. 1993; 69:351–360. [PubMed: 8497848]
31. Dharmasiri K, Smith DL. Mass spectrometric determination of isotopic exchange rates of amide hydrogens located on the surfaces of proteins. *Anal Chem*. 1996; 68:2340–2344. [PubMed: 8686927]
32. Balasubramaniam D, Komives EA. Hydrogen-exchange mass spectrometry for the study of intrinsic disorder in proteins. *Biochim Biophys Acta*. 2013; 1834:1202–1209. [PubMed: 23099262]
33. Truhlar SM, Torpey JW, Komives EA. Regions of I B that are critical for its inhibition of NF- B-DNA interaction fold upon binding to NF- B. *Proc Natl Acad Sci U S A*. 2006; 103:18951–18956. [PubMed: 17148610]
34. Keppel TR, Howard BA, Weis DD. Mapping unstructured regions and synergistic folding in intrinsically disordered proteins with amide H/D exchange mass spectrometry. *Biochemistry*. 2011; 50:8722–8732. [PubMed: 21894929]
35. Devarakonda S, Gupta K, Chalmers MJ, Hunt JF, Griffin PR, Van Duyne GD, Spiegelman BM. Disorder-to-order transition underlies the structural basis for the assembly of a transcriptionally active PGC-1 /ERR complex. *Proc Natl Acad Sci U S A*. 2011; 108:18678–18683. [PubMed: 22049338]
36. Balasubramaniam D, Komives EA. Hydrogen-exchange mass spectrometry for the study of intrinsic disorder in proteins. *Biochim Biophys Acta*. 2013; 1834:1202–1209. [PubMed: 23099262]
37. Tsutsui Y, Kuri B, Sengupta T, Wintrode PL. The structural basis of serpin polymerization studied by hydrogen/deuterium exchange and mass spectrometry. *J Biol Chem*. 2008; 283:30804–30811. [PubMed: 18794298]
38. Janmey PA, Ferry JD. Gel formation by fibrin oligomers without addition of monomers. *Biopolymers*. 1986; 25:1337–1344. [PubMed: 3741996]
39. Marx G. Protofibrin clots induced by calcium and zinc. *Biopolymers*. 1987; 26:911–920. [PubMed: 3607248]
40. Doolittle RF, Pandi L. Binding of synthetic B knobs to fibrinogen changes the character of fibrin and inhibits its ability to activate tissue plasminogen activator and its destruction by plasmin. *Biochemistry*. 2006; 45:2657–2667. [PubMed: 16489759]

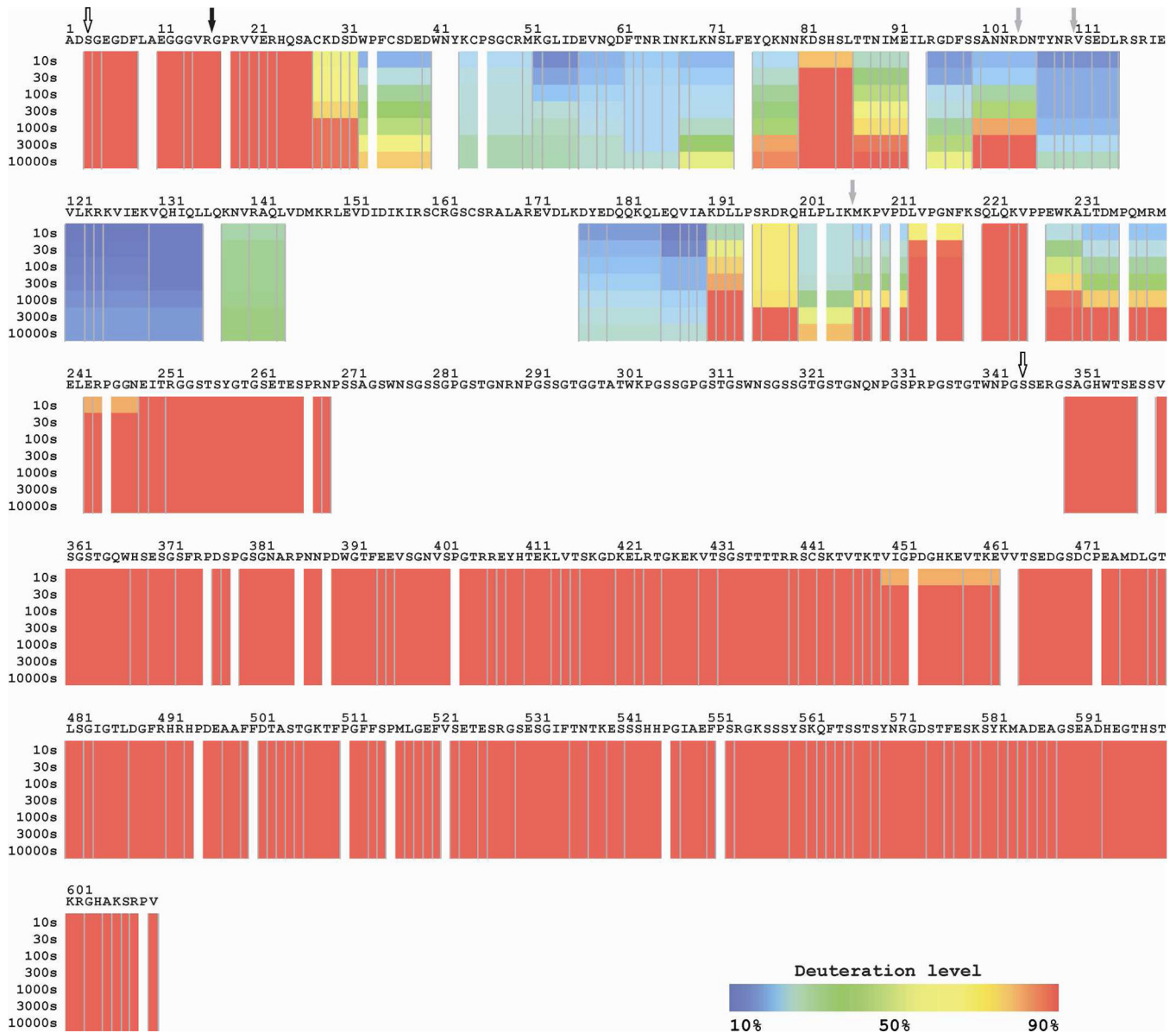
41. Medved L, Nieuwenhuizen W. Molecular mechanisms of initiation of fibrinolysis by fibrin. *Thromb Haemost*. 2003; 89:409–419. [PubMed: 12624622]

**Figure 1.**

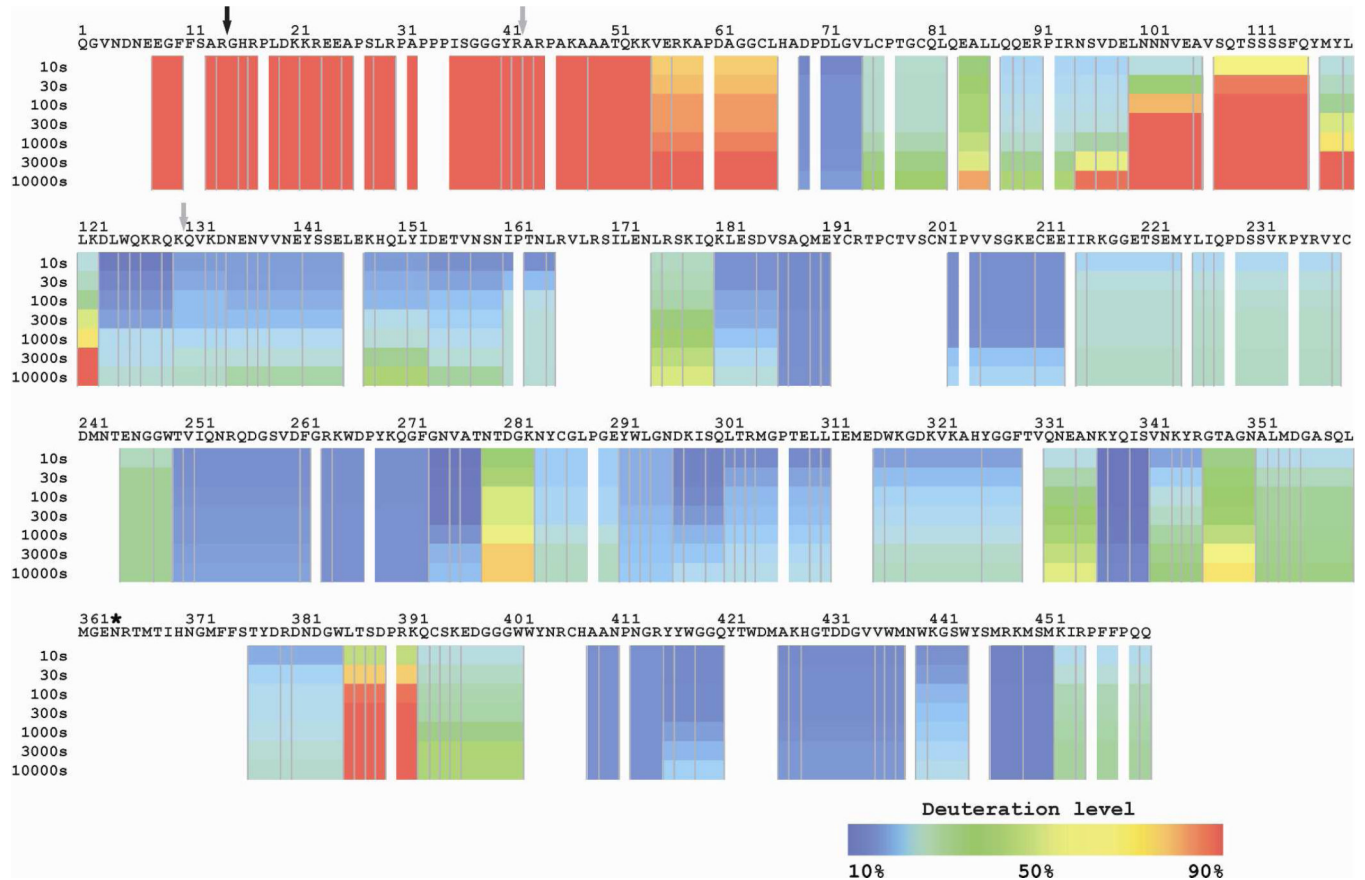
Analysis of purified normal fibrinogen. *Panel A*: Fibrinogen purity was assessed by SDS PAGE on 4–12% polyacrylamide gels under reducing (R) and non-reducing (NR) conditions (1.5 μ g per lane). The migration of intact fibrinogen (Fgn) as well as the constituent A α , B β , and γ chains is shown. Mass standards (in kDa) are shown on the left. Fibrinogen purity was >95% based on densitometric scanning of the stained gel. *Panel B*: Standard liquid chromatography-mass spectrometry analysis of reduced and denatured fibrinogen showing nonphosphorylated (P0), mono-phosphorylated (P1) and di-phosphorylated isoforms of the A α chain (*top*), and the mono-sialylated (S1) and di-sialylated (S2) isoforms of the B β chain (*middle*), and γ chain (*bottom*).

**Figure 2.**

Abbreviated peptide coverage maps for the A (*panel A*), B (*panel B*), and (*panel C*) chains of deuterated fibrinogen. Fibrinogen was incubated in the absence and presence of deuteration buffer and then quenched with a solution containing 6.4 M guanidine HCl and 1.0 M TCEP followed by proteolytic fragmentation with pepsin and fungal proteases, and mass spectrometry analysis as described in Experimental Procedures. Only those peptides identified in the non-deuterated, functionally-deuterated, and equilibrium-deuterated states are shown (maximum of 12 peptides per cascade). The amino acid sequences of the A, B, and chains of circulating fibrinogen were taken from GenBank accession numbers NP_068657, NP_005132, and NP_000500, respectively.

**Figure 3.**

Deuterium exchange profile of the fibrinogen A₁ chain after on-exchange at 0°C. The deuteration level at each time point is indicated below the amino acid sequence as a colored bar (see inset). On-exchange times are indicated to the left of the sequence. Gaps at proline residues result from absence of amide hydrogen. Vertical lines indicate the ends of overlapping peptides used to calculate deuteration levels. The thrombin cleavage site (black arrow), the plasmin cleavage sites (gray arrows), and the *in vivo* phosphorylation sites (white arrows) are shown above the amino acid sequence.

**Figure 4.**

Deuterium exchange profile of the fibrinogen B chain after on-exchange at 0°C. The deuteration level at each time point is indicated below the amino acid sequence as a colored bar (see inset). On-exchange times are indicated to the left of the sequence. The thrombin cleavage site (*black arrow*), the plasmin cleavage sites (*gray arrows*), and the oligosaccharide attachment site (*asterisk*) are shown above the amino acid sequence. See the legend to Figure 3 for additional details.

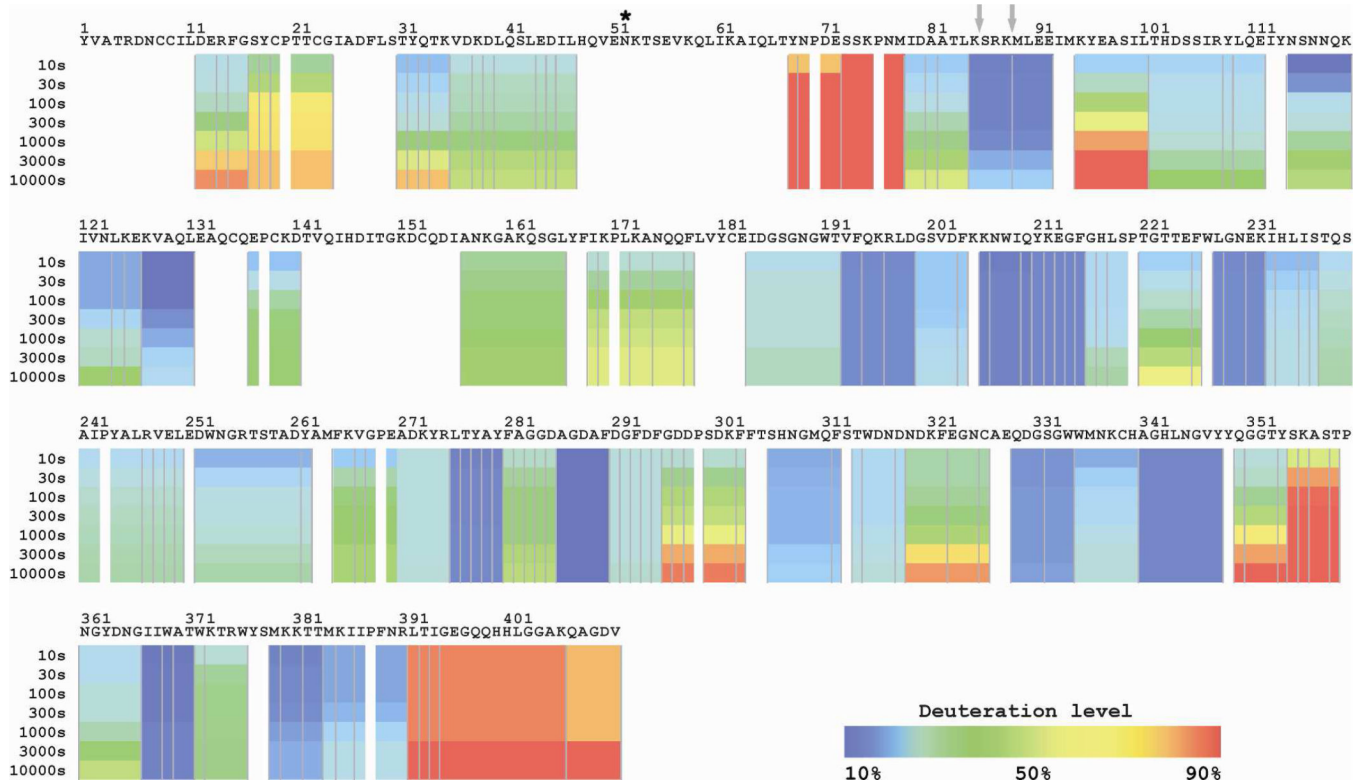


Figure 5.
 Deuterium exchange profile of the fibrinogen chain after on-exchange at 0°C. The deuteration level at each time point is indicated below the amino acid sequence as a colored bar (see inset). On-exchange times are indicated to the left of the sequence. Plasmin cleavage sites (gray arrows) and the oligosaccharide attachment site (asterisk) are shown above the amino acid sequence. See the legend to Figure 3 for additional details.

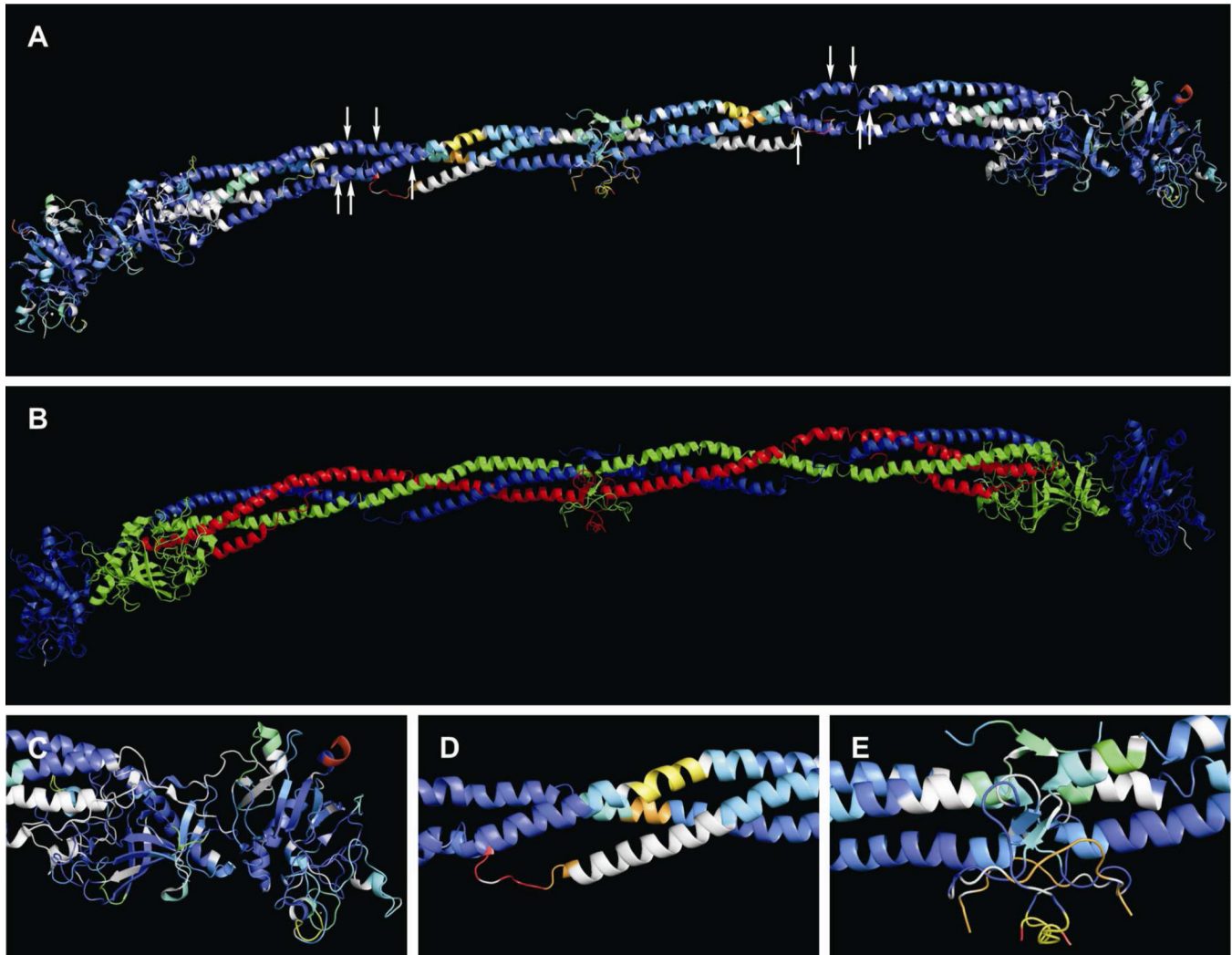


Figure 6.

Crystal structure of human fibrinogen (PDB entry 3GHG)⁶ as represented by the 10-second deuterium on-exchange profile. *Panel A:* The A₁, B₁ and B₂ chains of fibrinogen are color-coded according to the 10-second deuterium exchange profile of the respective chains (see Fig. 3 inset for interpretation of deuteration color codes). Deuteration gaps are colored white. Plasmin cleavage sites in the coiled-coil regions are denoted by white arrows. *Panel B:* For comparison, the same fibrinogen structure color-coded according to chain: A (red), B (green), and C (blue). *Panels C–E:* Close ups of deuterated regions shown in *Panel A*; terminal globular region on the right side of the molecule (*Panel C*), coiled-coil region on the left side of the molecule (*Panel D*), and the central region (*Panel E*).

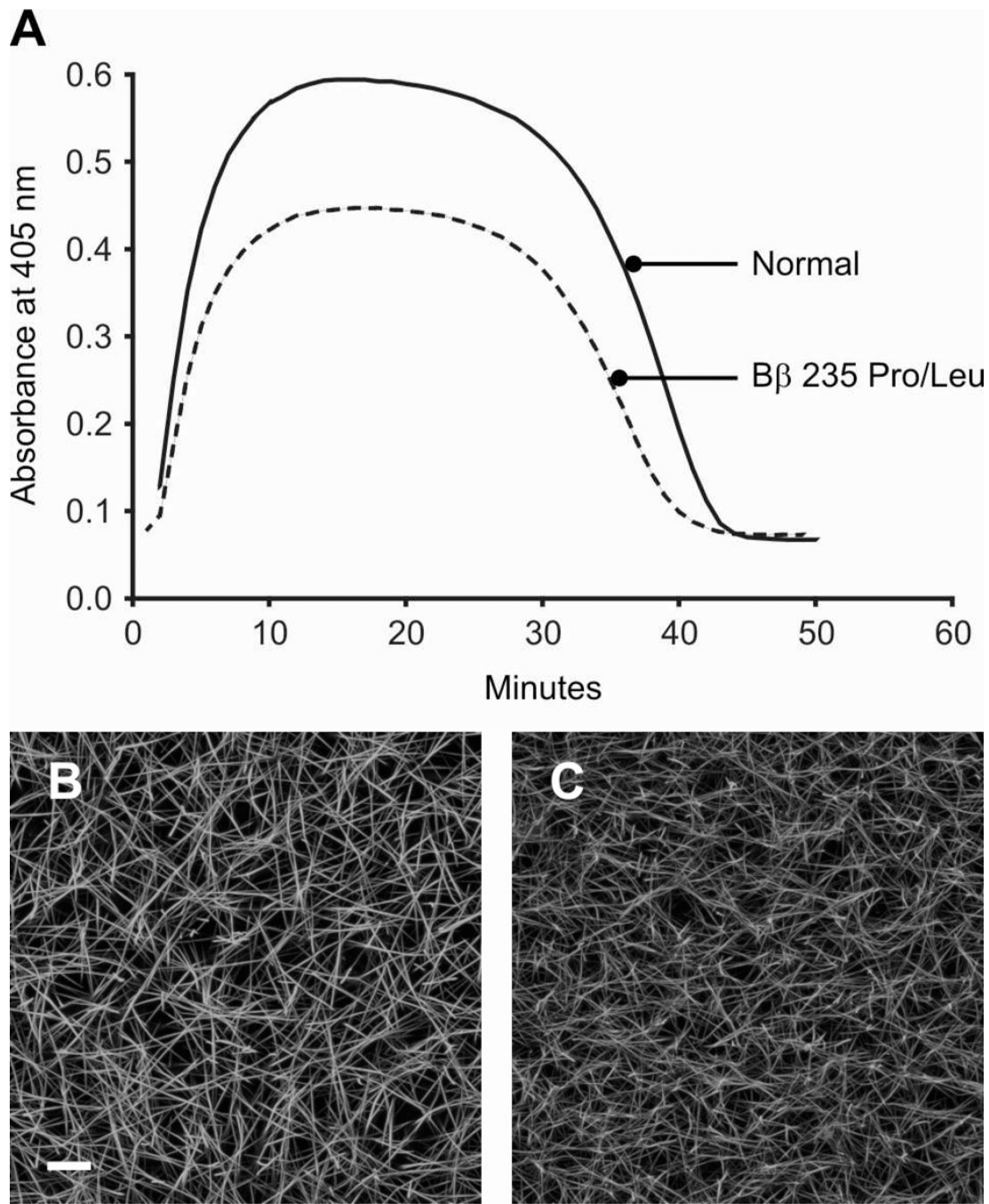
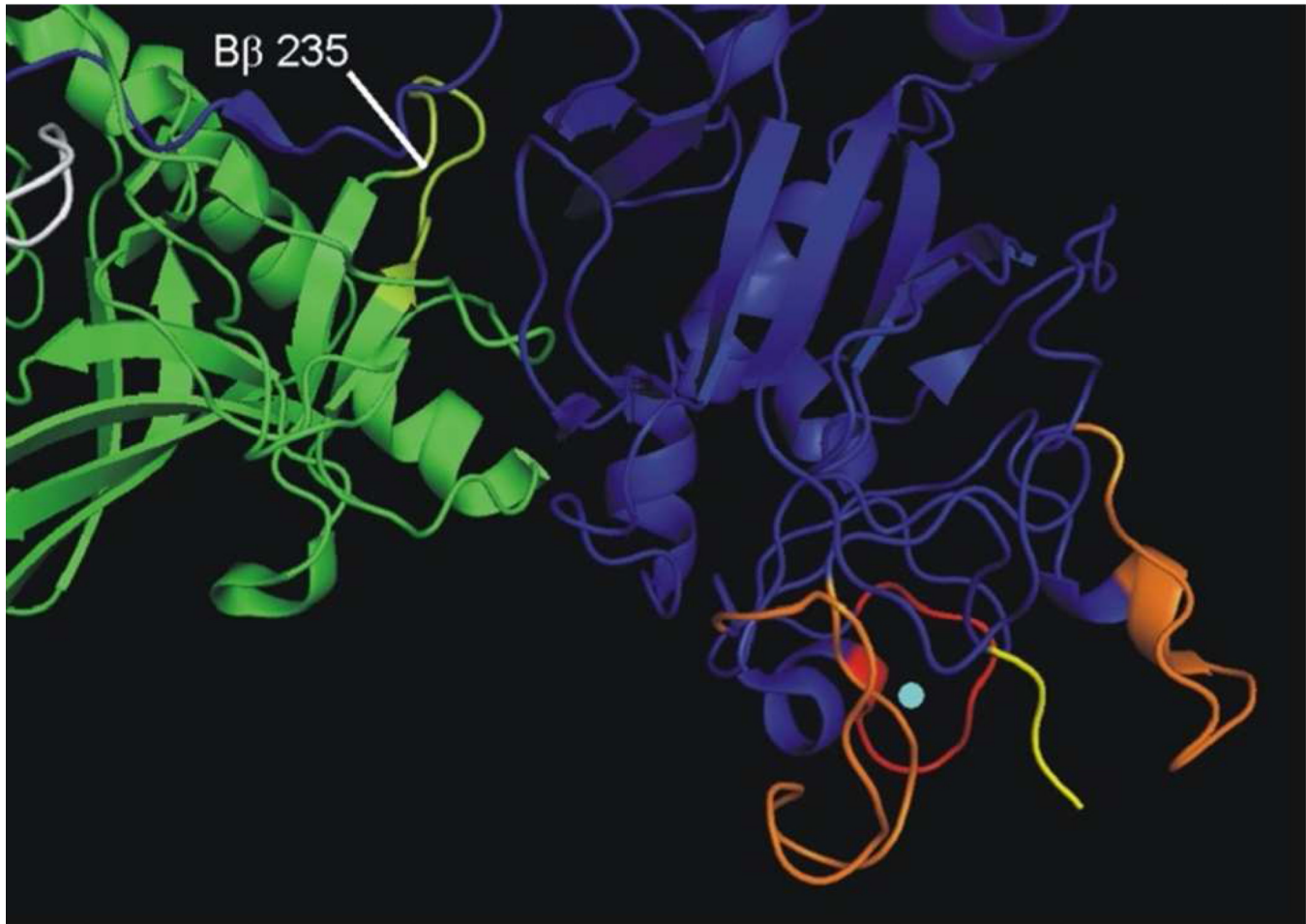
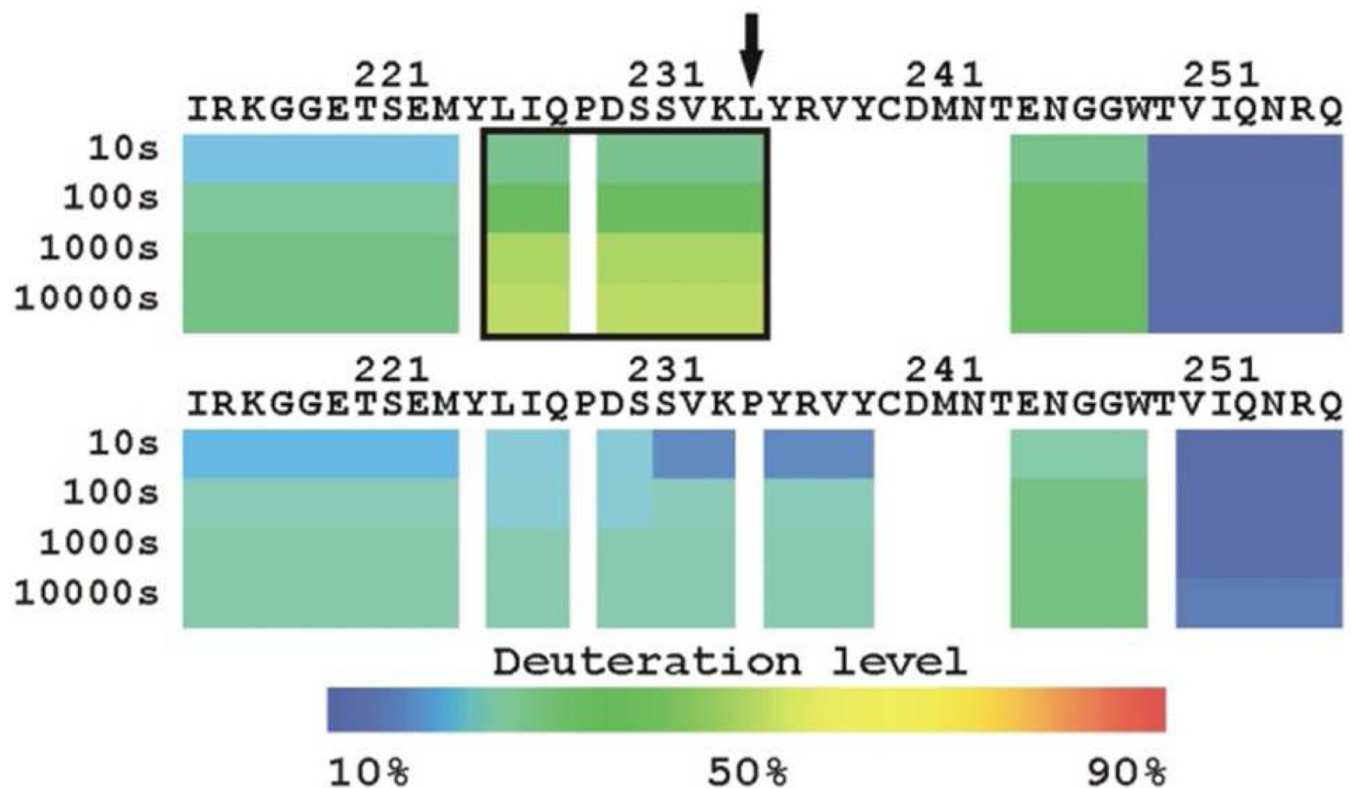


Figure 7.

Panel A: Turbidity curves showing polymerization and lysis of fibrin clots prepared from normal and B β 235 Pro/Leu fibrinogen. B β 235 Pro/Leu fibrinogen exhibits lower maximum turbidity and lysis rate. The experiment was repeated 3 times with similar results. Confocal micrographs of fibrin clots prepared from normal (*Panel B*) and B β 235 Pro/Leu (*Panel C*) fibrinogen. B β 235 Pro/Leu fibrinogen exhibits a more disorganized fibrin network structure characterized by thinner fibers, more branch points, and smaller pore size (confirmed by permeation studies). The experiment was repeated 5 times with similar results. Both micrographs are shown at 100X magnification. The scale bar in Panel B represents 10 μ m.

**Figure 8.**

Crystal structure of fibrinogen surrounding the B₂₃₅ Pro/Leu substitution site. The B₂₃₅ amino acid substitution occurs at the interface between the C domain (green) and the C domain (blue). The A knob synthetic peptide Gly-Pro-Arg-Pro-amide (yellow) is shown bound in the polymerization pocket within the C domain. The tightly bound calcium ion (cyan) in the C domain is also shown. Regions of enhanced deuterium exchange in B₂₃₅ Pro/Leu fibrinogen include a segment adjacent to the substitution site, (B_{226–235}, light green), a segment surrounding the calcium binding site (319–326, red), and 2 segments forming the walls of the polymerization pocket (291–303 and 350–366, orange).

**Figure 9.**

Deuterium exchange profile of B 235 Pro/Leu and normal fibrinogen surrounding the B 235 amino acid substitution site. The deuteration level of B 235 Pro/Leu fibrinogen (*top*) and normal fibrinogen (*bottom*) at each time point is indicated below the amino acid sequence as a colored bar (see inset). On-exchange times are indicated to the left of the sequence. Peptides containing leucine at amino acid 235 in B Pro/Leu fibrinogen exhibited enhanced deuterium exchange (*boxed region*) compared to normal fibrinogen. The amino acid substitution site is denoted by an *arrow*.

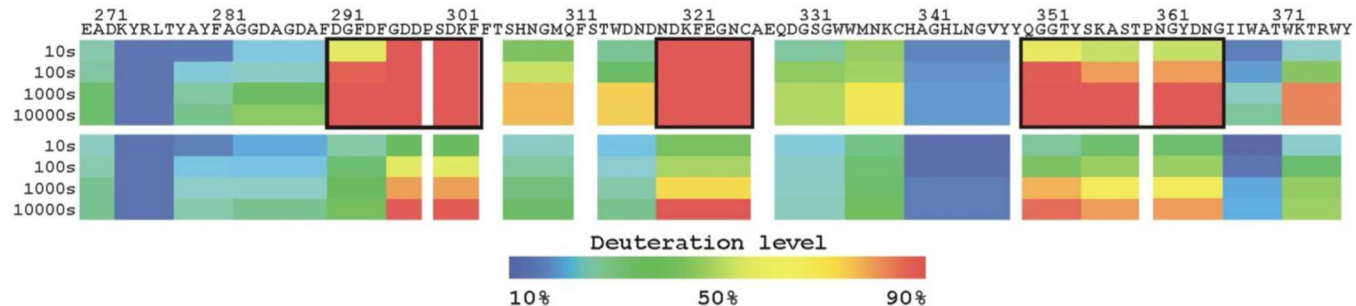


Figure 10.

Deuterium exchange profile of B 235 Pro/Leu and normal fibrinogen within the C domain. The deuteration level of B 235 Pro/Leu fibrinogen (*top*) and normal fibrinogen (*bottom*) at each time point is indicated below the amino acid sequence as a colored bar (see inset). On-exchange times are indicated to the left of the sequence. The C regions of enhanced deuterium exchange in B 235 Pro/Leu fibrinogen are boxed.

Table 1

Effect of protease treatment on fibrinogen fragmentation.^a

Chain (residues)	Protease	# of peptides	# of residues covered	% coverage
A (610)	Pepsin	414	570	93.4
	Fungal	411	435	71.3
	Pepsin + Fungal	587	572	93.7
B (461)	Pepsin	248	411	89.2
	Fungal	112	322	69.8
	Pepsin + Fungal	266	413	89.6
(411)	Pepsin	274	360	87.6
	Fungal	175	268	65.2
	Pepsin + Fungal	318	376	91.5

^aThe quench solution contained 0.5 M guanidine HCl and 0.05 M TCEP.

Effect of quench solution guanidine HCl and TCEP concentrations on fibrinogen fragmentation.^a

Table 2

Chain (residues)	Guanidine HCl (M)	TCEP (M)	# of peptides	# of residues covered	% coverage
A (610)	0.5	0.05	587	572	93.7
	6.4	1.0	627	572	93.7
B (461)	0.5	0.05	266	413	89.6
	6.4	1.0	324	444	96.3
(411)	0.5	0.05	318	376	91.5
	6.4	1.0	306	376	91.5

^aBoth pepsin and fungal proteases were used for fragmentation.

Table 3

Properties of fibrin clots prepared from B 235 Pro/Leu and normal fibrinogen.^a

Clot property	Fibrinogen		
	B 235 Pro/Leu	Normal	P value ^b
Turbidity (absorbance units)	0.360 ± 0.054	0.482 ± 0.045	<0.05
Lysis rate (milli-absorbance units per min)	31.9 ± 3.7	41.8 ± 1.3	<0.05
Fiber diameter (nm)	455 ± 4	535 ± 10	<0.01
Fiber branching (branch points per field) ^c	863 ± 127	614 ± 131	<0.01
Darcy constant, K _s ($\times 10^{10}$)	3.42 ± 0.26	7.65 ± 0.14	<0.001

^aData are presented as mean ± SD of 3–5 experiments.

^bTwo-sided t test.

^cField dimensions were 127×127×0.76 μm.